JOURNAL OF SOLID STATE CHEMISTRY 104, 377–390 (1993)

Crystal Chemistry and Magnetism of Ternary Actinoid Boron Carbides $UB_{1-x}C_{1+x}$ and $U_{1-x}M_xB_2C$ with M = Sc, Lu, and Th

P. ROGL,* B. RUPP, *,† I. FELNER,‡ AND P. FISCHER¶

*Institut für Physikalische Chemie der Universität Wien, Währingerstraße 42, A-1090 Vienna, Austria; †Lawrence Livermore National Laboratory, University of California, POB 808, Livermore, California 94550; ‡Racah Institute of Physics, The Hebrew University, Jerusalem IL-91904, Israel; and ¶Laboratorium für Neutronenstreuung, Eidgenössische Technische Hochschule Zürich und Paul Scherrer Institut, CH-5232 Villigen, PSI, Switzerland

Received June 8, 1992; accepted October 29, 1992

Within the homogeneous range of uranium monocarbide $UB_{1-x}C_{1+x}$, the crystal structures of stoichiometric UBC and of the carbon-rich solid solution $UB_{0.78}C_{1.22}$ have been refined from single-crystal X-ray counter data. From X-ray analysis crystal symmetry in both cases is consistent with the centrosymmetric space group *Cmcm* and there are no indications of superstructure formation. In contrast to the fully ordered atom arrangement revealed for stoichiometric UBC (a = 0.35899(4), b = 1.19781(12), c = 0.33474(3) nm), random occupation by boron and carbon atoms is observed for the boron site in $UB_{0.78}C_{1.22}$ (a = 0.35752(4), b = 1.18584(3), c = 0.33881(4) nm). For 279(278) reflections ($|F_0| > 3\sigma$) the obtained reliability factors $R_x = \Sigma|\Delta F|/\Sigma\ |F_0|$ were R_x = 0.069 for UBC and R_x = 0.050 for $UB_{0.78}C_{1.22}$. Neutron powder diffraction experiments at 9 and 295 K unambiguously revealed full occupancy by the nonmetal atoms in $UB_{0.78}C_{1.22}$ and prove the statistical occupation of B and C atoms in the B-sites. For the orthorhombic symmetry *Cmcm*, refinement was not better than R_I = 0.044. A model calculation in monoclinic symmetry $C12/m1$, however, resulted in a significant reduction of the residual value to R_I = 0.030, releasing spatial constraints on the boron atoms. Thus the boron–boron chain in *Cmcm* (B–B = 0.1874 nm) is dissolved into boron pairs (B–B = 0.1706 nm) which are loosely bound at a distance of 0.2043 nm. The formation of C–B–B–C groups corresponds to the structure types of ThBC and $Th_3B_2C_3$. The magnetic behavior has been investigated in the temperature range from 4.2 K to 1000 K for $UB_{1-x}C_{1+x}$ (UBC-type) and $U_{1-x}M_xB_2C$ (ThB_2C-type for the high temperature modification and 1-UB_2C-type for the low temperature modification) with U partially substituted by Th or Sc, Lu. From magnetic susceptibilities, the alloys $UB_{1-x}C_{1+x}$ reveal temperature independent paramagnetism with typical intermediate valence fluctuation behavior (T_{SF} ~ 350 K). ThB_2C and 1-UB_2C both are temperature independent paramagnets, whereas h-UB_2C is a ferromagnet with the rather high Curie temperature T_M = 80(2) K. T_M and the saturation magnetiziation per U atom both successively decrease on substitution of U by Th, Sc, or Lu in UB_2C, whereas the U-moments remain practically unchanged at $\mu_{eff}(U) \sim 1.9\ \mu_B$. Uranium L_3-XANES (X-ray Absorption Near Edge Structure) spectroscopy revealed increased d-band localization, comparable to uranium–transition metal alloys, in nonmagnetic $UB_{1-x}C_{1+x}$ (x = 0, 0.22). No superconductivity was observed down to 1.5 K; no hydrogen uptake was observed for UB_2C and ThB_2C even under hydrogen pressures as high as 7×10^7 Pa at 670 K.

1. Introduction

Investigation of the uranium–boron–carbon system (*1*) essentially confirmed the existence of the actinoid monoboroncarbide with an extended region of homogeneity, and revealed the formation of two new compounds, UB_2C and $U_5B_2C_7$. The existence of orthorhombic UBC was first described by Matterson *et al.* (*2*) and it was later shown by Toth *et al.* (*3*) from X-ray powder intensity data to derive from the closely related structure types of CrB or $ZrSi_2$. At that time, however, no precise information

0022-4596/93 $5.00

TABLE I

MAGNETIC DATA FOR (U, Th, *RE*) BORON CARBIDES

Compound	Lattice Parameters in nm			$\mu_{(sat)}/U$ (μ_B)	$\mu_{(par)}/U$ (μ_B)	T_M (K)	Asymptotic Curie temperature (K)	Type of order
	a	*b*	*c*					
ThB_2C	0.66995(11)	—	1.14467(48)	—	—	—	—	weak PM, FM imp.
UB_2C, h.t.	0.65224(18)	—	1.07909(29)	0.64(3)	1.89(5)	80(2)	74(2)	FM
$U_{0.85}Sc_{0.15}B_2C$	0.65047(8)	—	1.05757(76)	0.57(3)	1.78(5)	63(2)	59(3)	FM
$U_{0.85}Lu_{0.15}B_2C$	0.65337(15)	—	1.07332(41)	0.20(2)	2.01(5)	58(2)	14(5)	FIM?
$U_{0.85}Th_{0.15}B_2C$	0.65499(7)	—	1.08448(20)	0.39(2)	1.82(5)	60(2)	60(3)	FM
$U_{0.70}Th_{0.30}B_2C$	0.65641(17)	—	1.09244(15)	0.38(2)	1.88(5)	35(2)	25(3)	FM
$U_{0.40}Th_{0.60}B_2C$	0.66054(13)	—	1.11318(15)	0.04(1)	2.17(9)	15(2)	−121(5)	weak FM, imp. ?
UB_2C, l.t.	0.60338(3)	0.35177(2)	0.41067(2)	—	—	—	—	weak PM, traces of h. t. UB_2C
UBC (32/35/33at%)	0.35908(5)	1.19957(16)	0.33470(4)	—	—	—	—	ICF,
UBC (32/32/36at%)	0.35899(4)	1.19781(12)	0.33473(3)	—	—	—	—	contains traces of
UBC (32/29/39at%)	0.35845(4)	1.18961(13)	0.33646(4)	—	—	—	—	h.t. UB_2C

Notes. h.t., high temperature modification; l.t., low temperature modification; ICF, inter valence fluctuations; PM, paramagnetic state; FIM, ferrimagnetic order; FM, ferromagnetic order.

was given (*3*) on the nonmetal occupation or nonmetal ordering throughout the homogeneous region.

The compound UB_2C has been observed (*1*) to exist in two modifications with a transition temperature of 1675°C. While the crystal structure of h-UB_2C was found to be isostructural with the recently described structure type of ThB_2C (*4*), the crystal structure of l-UB_2C is unique (*5*) and has not been observed with homologous actinoid elements. The crystal structure of "$U_5B_2C_7$," although recognized to be related to that of UC_2, has not been refined yet (*1*).

The lattice dimensions and interatomic distances of the various uranium boron carbides are close to the Hill limit (*6*), suggesting interesting magnetic and/or superconducting behavior, which served to motivate the present study of the structural and magnetochemical properties.

2. Experimental

Samples with nominal compositions given in Table I, each of a total amount of ca. 1 g, were prepared by arc-melting the elements together on a water cooled copper hearth, using a nonconsumable tungsten electrode in a protective Ti/Zr-gettered high purity argon atmosphere. Uranium platelets of nuclear grade (E. Merck, Darmstadt) were surface cleaned prior to use in dilute HNO_3; thorium was in the form of arc-melted buttons prepared from powder as obtained from Cerac Inc. with a claimed purity of 99.8%; 3N-rare earths (Sc, Lu) were in form of ingots (Auer–Remy, Hamburg); reactor grade carbon (impurities <1.4 ppm, Carbonne Lorraine, France) and boron (from H. C. Starck, Goslar, 99.8%) were used as powders which prior to arc-melting were compacted into small tablets. Weight losses were small and usually found to be within 0.5 wt.%. Due to the congruent melting behavior of h-UB_2C (stable above T = 1675°C; see Ref. (*1*)) h-$U_{1-x}M_xB_2C$ alloys were used for further investigations in the as cast condition. Practically single phase l-UB_2C and $U_{1-x}M_xB_2C$ with minor amounts of untransformed h-UB_2C was obtained after heat treatment of the alloy buttons for 75 hr at 1600°C in a W sheet metal high vacuum furnace (10^{-4} Pa) on a W substrate. The remaining samples of ThB_2C and $UB_{1-x}C_{1+x}$ were annealed under similar conditions for 120 hr at 1400°C and finally radiation quenched.

Precise lattice parameters and standard deviations (Table I) were obtained by least-squares refinement of room temperature

Guinier–Huber X-ray powder data, using monochromatic Cu$K\alpha_1$-radiation with an internal standard of 99.9999% pure Ge (a_{Ge} = 0.5657906 nm).

The $UB_{0.78}C_{1.22}$ sample (15 g) used for the neutron diffraction experiments was prepared as described above, but with 98.15% ^{11}B-enriched isotope from AERE Harwell, UK, impurities <6000 ppm.

Neutron powder diffraction was performed by means of the multidetector powder diffractometer with neutron wavelength $\lambda = 0.17012$ nm (resolution $\Delta d/d \geq 4 \times 10^{-3}$ (see Ref. 7)) at the 10-MW Saphir reactor in Villigen (PSI), Switzerland. Preferred orientation effects were minimized by powdering the sample to a grain size smaller than 25 μm in a He-filled glove box. Further details concerning the experiment are summarized in Table II. Atom distribution, precise atom parameters and occupancies, individual thermal factors, and profile parameters were derived from a least-squares powder profile refinement (*8*) using the neutron scattering lengths of a recent compilation by Sears (*9*). A series of reliability measures, which are defined in detail in Table I, was calculated. The observed powder diffractogram, containing small amounts of UC as a secondary equilibrium phase, is shown in Fig. 1.

Rather small but isodimensional single crystal fragments were broken from needles or briquettes, selected by mechanical fragmentation of the arc melted UBC and the $UB_{0.78}C_{1.22}$ alloy buttons respectively. X-ray intensity data were collected on an automatic STOE four-circle diffractometer in one hemisphere of the reciprocal space out to a limit of $\sin\theta/\lambda = 9.0$ nm^{-1} using monochromatized Mo$K\alpha$- radiation. Sets of 281 (282) symmetry independent reflections were obtained for UBC and $UB_{0.78}C_{1.22}$, respectively, by averaging symmetry equivalent reflections out of a total number of 2012 (2015) recorded intensities; all observed intensities [279 (278) for $|F_0| > 3\sigma(F_0)$] were used in the structure refinement. An empirical absorption correction was applied, using ψ-psi scans of four independent reflections. The crystallographic data are summarized in Table III. Analyses of Weissenberg photographs (axes [001] and [101]) revealed an orthorhombic lattice geometry without any indications of superstructure formation; a center of symmetry was displayed from statistical tests. The only sets of extinctions observed were (hkl) for $h + k = 2n$ and ($h0l$) for $h, l = 2n$; this observation is essentially consistent with the centrosymmetric type of space group $Cmcm$ and/or the noncentrosymmetric $Cmc2_1$ and confirms earlier findings from X-ray powder data of UBC (*3*).

Magnetic data were recorded in the range $4.2 < T < 300$ K with a P.A.R. vibrating sample magnetometer. For measurements from 77 to 1000 K a compensating high precision Faraday pendulum magnetometer (SUS 10, A. Paar K. G., Austria) was used. In the paramagnetic region the magnetic moment μ_{eff}, the paramagnetic Curie–Weiss temperature θ_p, and the temperature independent part of the susceptibility χ_0 (including core diamagnetism, Pauli paramagnetism, and second order van Vleck terms) were obtained as final parameters of a nonlinear least squares minimization of the Curie–Weiss law

$$\chi_m = \frac{N\mu^2}{3\,k_B\,(T-\theta)} + \chi_0$$

where χ_m is the measured total mol-susceptibility, N is Avogadro's number and k_B is Boltzmann's constant.

Uranium L_3-edge XANES spectra were recorded on beamline X-11A at the Brookhaven National Synchrotron Light Source. The X-ray storage ring was operated at 2.53 GeV with electron beam currents of 120 to 160 mA. Silicon (111) monochromator crystals were used in combination with entrance slit widths of 0.25 mm to provide an energy resolution of about 2 eV at 17.2 keV. Powders of sample material were sealed in Kaptan tape to obtain transmission samples of uniform thickness corresponding to 1 to 1.5 absorption lengths. The samples were examined using the conventional transmission technique with an energy scan step size

TABLE II

EXPERIMENTAL DATA FOR $UB_{0.78}C_{1.22}$

Sample container	Vanadium double cylinder, R_a/R_i= 5/4 mm
Temperature (K)	296 K
Radiation, wavelength (nm)	Neutrons, λ = 0.17012(1)
Absorption correction	μ_D = 0.241
Reactor	Saphir, PSI CH-Villigen
Monochromator	Germanium-(311)
Soller slits	10'/–/12'
2θ – range (2 θ)	3.0 to 134.9
Step – scan increment (2 θ)	0.10
Coherent scattering lengths (fm)	U 8.417
	B 6.646
	C 6.646
Number of contributing reflections	119
Background	Background refinement (6 parameters)
Preferred orientation	[001]
Number of variables	26
Largest element of correlation matrix	0.7
Maximal Δ/σ	<0.01
R – Values:	
$R_I = \lvert I_i\,(\text{obs}) - (1/c)\,I_i\,(\text{calc})\rvert/\sum I_i\,(\text{obs})$	
$R_F = \lvert[I_i\,(\text{obs})]^{1/2} - [I_i\,(\text{calc})]^{1/2}\rvert/\sum [I_i\,(\text{obs})]^{1/2}$	
$R_P = \lvert Y_i\,(\text{obs}) - (1/c)\,Y_i\,(\text{calc})\rvert/\sum Y_i\,(\text{obs})$	
$R_{WP} = [\sum w_i\lvert Y_i\,(\text{obs}) - (1/c)\,Y_i\,(\text{calc})\rvert^2/\sum w_i\lvert Y_i\,(\text{obs})\rvert^2]^{1/2}$	
$R_e = \{(N - P + C)/\sum w_i\,Y_i\,(\text{obs})\}^{1/2}$	
$\chi^2 = \{R_{wp}/R_e\}$	
I_i Integrated intensity of reflection i	
w_i Weighting function	
Y_i Number of counts (background corrected) at 2θ	
c Scale factor	

of 0.5 eV. Freshly cleaned uranium foil (2 absorption lengths) was simultaneously scanned as an energy reference during each measurement.

3. Results and Discussion

3.1. The Crystal Structures of UBC and $UB_{0.78}C_{1.22}$

3.1.1. X-ray diffraction. The prominent peaks of a three dimensional Patterson map $P(u, v, w)$ were all found to be compatible with 4U in the 4c-sites of the centrosymmetric space group *Cmcm*. A difference Fourier map $F_0 - F_U$ clearly resolved the nonmetal atom sites to be four boron atoms in 4c and four carbon atoms in 4c, thereby confirming the structure model as earlier derived for UBC from X-ray powder data (*3*). Assuming these data as starting parameters, the intensity data for both single crystals UBC and $UB_{1-x}C_{1+x}$ were refined using the STRUCSY full matrix least-squares program system (STOE & Cie., Darmstadt). The weights used were based upon counting statistics $w_i = 1/\sigma(F_i)^2$, and structure factors were furthermore corrected for isotropic secondary extinction; different weighting schemes had no significant influence on the R-values obtained. Refinement of the occupancy of the uranium atoms did not result in a significant deviation from full occupation. Due to the small X-ray scattering power of the nonmetal atoms, model calculations were carried out with (a) interchanged atom positions, (b) partially occupied nonmetal sites, and (c) random distributions on the

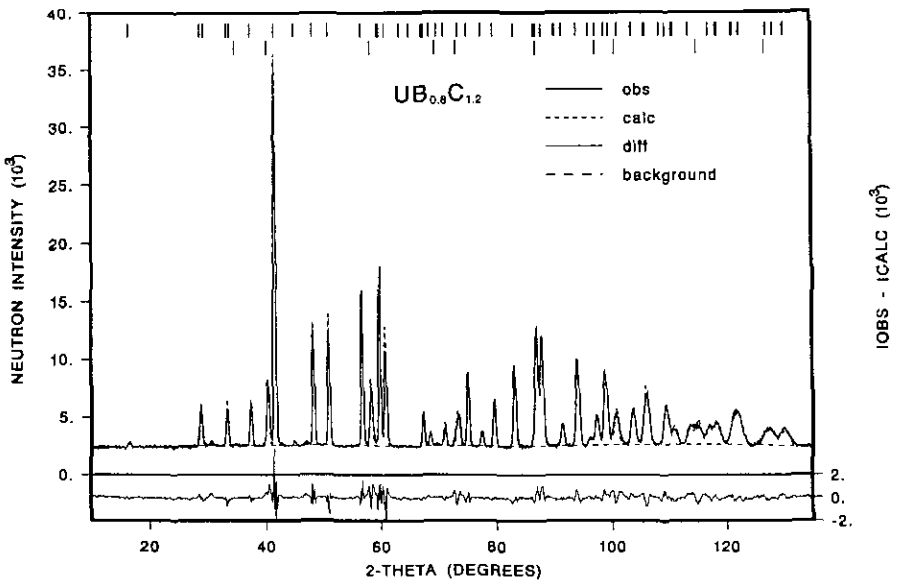

FIG. 1. Observed (solid line) and calculated (broken line) neutron powder diffraction pattern of $UB_{0.78}C_{1.22}$ at 9 K; $\lambda_n = 0.17012$ nm. Bragg positions of $UB_{0.78}C_{1.22}$ and of UC reflections are indicated by vertical bars in two top lines. Refinement in monoclinic symmetry $C12/m1$ (see Table III).

individual nonmetal sites; all unambigously resulted in a fully ordered atom arrangement for stoichiometric UBC and a statistical occupation of B,C-atoms in the B-sites in carbon-rich $UB_{0.78}C_{1.22}$ (see Table III and Section 3.1.2.).

The final R-values calculated with anisotropic thermal parameters for the uranium atoms were $R = 0.069$ for UBC and $R = 0.050$ for $UB_{0.78}C_{1.22}$. The final positional and thermal parameters are given in Table III; for interatomic distances, see Table IV. A listing of F_0 and F_c values can be obtained on request.

3.1.2. Neutron powder diffraction of $UB_{0.78}C_{1.22}$. Refinements of the neutron data for $UB_{0.78}C_{1.22}$ at 295 K and 9 K, based on the structure model obtained from the X-ray analysis with orthorhombic symmetry *Cmcm*, were no better than $R_I = 0.044$; however, they proved the full occupation of the nonmetal sites as well as the statistical distribution of B,C atoms on the B-sites (Table III).

A significant decrease of the residual value to $R_I = 0.030$ can be achieved by transferring the structure model to the monoclinic subgroup $C12/m1$, thereby releasing the spatial constraints on the boron atoms. It shall be mentioned that the corresponding refinement of the unit cell dimensions in $C2/m$ did not reveal any deviations from the orthorhombic lattice geometry; i.e., the obviously monoclinic nonmetal sublattice does not alter the orthorhombicity of the unit cell (within the limits of the standard deviations). Besides some small amounts of UC, which were refined as a second phase, there were no extra peaks detectable from the neutron data, confirming the absence of superstructures (see also Fig. 1). Due to the identical neutron scattering lengths of ^{11}B and C, atom ordering within the nonmetal sublattice, however, cannot be monitored employing neutron diffraction techniques.

The final structural and profile parameters, as well as the residual values obtained from the least squares refinement, including

TABLE III

CRYSTALLOGRAPHIC DATA FOR UBC AND $UB_{0.78}C_{1.22}$ (UBC-TYPE)

X-ray single crystal data at 295 K, $\lambda = 0.07071$ nm
Space group, $Cmcm - D_{2h}^{17}$, No. 63, , $Z = 4$; origin at center. The expression for the individual isotropic temperature factor is $T = \exp(-B(\sin\theta/\lambda)^2) = \exp(-2\pi^2 U_{iso}(\sin\theta/\lambda)^2)$.
Anisotropic thermal factors are expressed as $T = \exp(-2\pi^2(U_{11}h^2a^{*2} + U_{22}k^2b^{*2} + U_{33}l^2c^{*2} + 2U_{12}hka^*b^* + 2U_{13}hla^*c^* + 2U_{23}klb^*c^*)$. By symmetry $U_{12} = U_{13} = U_{23} = 0$. The standard deviations are in parentheses.

(I) The crystal structure of stoichiometric UBC

Atom	Site	x	y	z	Occ.	$U_{11}(U_{iso})$	U_{12}	U_{13}
U	4c	0	0.1386(2)	$\frac{1}{4}$	1.0	0.011(1)	0.005(1)	0.003(1)
B	4c	0	0.4624(47)	$\frac{1}{4}$	1.0	0.007(9)	—	—
C	4c	0	0.3357(42)	$\frac{1}{4}$	1.0	0.007(8)	—	—

$a = 0.35899(4)$, $b = 1.19781(12)$, $c = 0.33473(3)$ nm; $c/a = 0.932$, $b/a = 3.337$; $V = 0.1439$ nm^3;
$\rho_x = 12.03$ Mg m^{-3}, $\mu(MoK\alpha) = 107.3$ mm^{-1}.
Correction for isotropic secondary extinction was $g = 1.6 \times 10^{-6}$.
Reliability factors: $R_F = 0.069$, $R_w = 0.069$.

(II) The crystal structure of $UB_{0.78}C_{1.22}$

Atom	Site	x	y	z	Occ.	$U_{11}(U_{iso})$	U_{12}	U_{13}
U	4c	0	0.1381(1)	$\frac{1}{4}$	1.0	0.013(1)	0.005(1)	0.008(1)
B, C1	4c	0	0.4648(30)	$\frac{1}{4}$	0.78 0.22	0.015(5)	—	—
C2	4c	0	0.3355(23)	$\frac{1}{4}$	1.0	0.011(4)	—	—

$a = 0.35752(4)$, $b = 1.18584(3)$, $c = 0.33881(4)$ nm; $c/a = 0.948$, $b/a = 3.317$; $V = 0.1436$ nm^3;
$\rho_x = 12.08$ Mg m^{-3}, $\mu(MoK\alpha) = 107.1$ mm^{-1}.
Correction for isotropic secondary extinction was $g = 2.8 \times 10^{-6}$.
Reliability factors: $R_F = 0.050$, $R_w = 0.050$.

Neutron powder diffraction at 295 K, $\lambda = 0.17012$ nm.

(A) space group $Cmcm - D_{2h}^{17}$, No. 63

$a = 0.35835(3)$, $b = 1.19012(8)$, $c = 0.33692(3)$ nm; $c/a = 0.941$ $b/a = 3.321$ $V = 0.1437$ nm^3.

Atom	Site	x	y	z	Occ.	U_{11} (U_{iso})
U	4c	0	0.1379(2)	$\frac{1}{4}$	1.0	0.30(5)
B[11], C	4c	0	0.4648(2)	$\frac{1}{4}$	0.78 0.22	0.88(7)
C	4c	0	0.3346(3)	$\frac{1}{4}$	1.0	0.29(7)

Reliability factors: $R_I = 0.044$, $R_F = 0.030$, $R_{WP} = 0.064$, $R_e = 0.036$, $\chi^2 = 3.15$.

(B) space group $C12/m1 - C_{2h}^3$, No. 12

$a = 1.19013(8)$, $b = 0.35835(3)$, $c = 0.33692(3)$, $\beta = 90.0°$.

Atom	Site	x	y	z	Occ.	U_{11} (U_{iso})
U	4i	0.1378(2)	0	0.2500(–)	1.0	0.32(5)
B[11], C	4i	0.4657(2)	0	0.2752(4)	0.78 0.22	0.73(6)
C	4i	0.3352(2)	0	0.2603(4)	1.0	0.19(6)

Reliability factors: $R_I = 0.030$, $R_F = 0.028$, $R_{WP} = 0.062$, $R_e = 0.036$, $\chi^2 = 2.96$.

TABLE IV

INTERATOMIC DISTANCES (IN nm) FOR UBC AND $UB_{0.78}C_{1.22}$

X-ray diffraction		Neutron diffraction	
Stoichiometric UBC	$UB_{0.78}C_{1.22}$	$UB_{0.78}C_{0.22}$ – *Cmcm*, 9K	$UB_{0.78}C_{1.22}$ – *C*12/*m*1, 9K
U–2U 0.3720(3)	U–2U 0.3687(1)	U–2U 0.3681(4)	U–2U 0.3679(4)
–4U 0.3626(2)	–4U 0.3621(1)	–4U 0.3610(0)	–4U 0.3627(4)
–2U 0.3589(0)	–2U 0.3575(0)	–2U 0.3581(0)	–2U 0.3581(0)
–2U 0.3347(0)	–2U 0.3388(0)	–2U 0.3361(0)	–2U 0.3361(0)
–2B 0.277(4)	–2B 0.272(3)	–2B 0.2723(3)	–2B 0.2733(3)
–4B 0.274(3)	–4B 0.275(1)	–4B 0.2743(2)	–2B 0.2802(7)
–4C 0.247(1)	–4C 0.248(0)	–4C 0.2478(1)	–2B 0.2687(7)
–1C 0.236(5)	–1C 0.234(3)	–1C 0.2336(4)	–2C 0.2500(8)
			–2C 0.2455(8)
B–2U 0.277(4)	B–2U 0.272(3)	B–2U 0.2723(3)	–1C 0.2340(3)
–4U 0.274(2)	–4U 0.275(2)	–4U 0.2743(2)	
–2B 0.190(5)	–2B 0.189(3)	–2B 0.1874(2)	B^{II}–2U 0.2723(3)
–1C 0.152(7)	–1C 0.153(4)	–1C 0.1553(4)	–2U 0.2802(7)
			–2U 0.2687(7)
C–4U 0.247(1)	C–4U 0.247(0)	C–4U 0.2478(1)	– B 0.2043(20)
–1U 0.236(5)	–1U 0.234(3)	–1U 0.2336(4)	– B 0.1706(20)
–1B 0.152(7)	–1B 0.153(4)	–1B 0.1553(4)	– C 0.1553(3)
			C–1U 0.2340(3)
			–2U 0.2455(8)
			–2U 0.2500(8)
		B–B–B 127.5°	– B 0.1553(4)
		B–B–C 116.3°	
		B–B–C 116.3°	
			B–B–B 127.1°
			B–B–C 111.7°
			B–B–C 121.2°

simultaneous refinement of the background (*8*), are presented in Table III in comparison to the single crystal X-ray data. Atom distances are given in Table IV. As seen from Fig. 1 and from the residual values in Table III, observed and calculated neutron intensities are in excellent agreement. This is furthermore true for the X-ray powder intensity calculation employing the refined atom parameters from the neutron diffraction. The unit cell dimensions obtained for UC as the second but minor equilibrium phase were a = 0.49455(5) in the alloy with the $UB_{0.78}C_{1.22}$ phase: a = 1.19013(1), b = 0.35835(3), c = 0.33692(3) nm at 295 K and a = 0.49459(4) with $UB_{0.78}C_{1.22}$: a = 1.18835(9), b = 0.35807(3), c = 0.33611(3) nm at 9 K and compare well with the data earlier obtained from the investigation of the U–B–C ternary system (*1*).

3.1.3. The solid solutions $Th_{1-x}U_xB_2C$ and $U_{1-x}RE_xB_2C$ (RE = Sc, Lu). Guinier X-ray powder patterns of samples $Th_{1-x}U_xB_2C$ (x = 0.4, 0.7, and 0.85), as cast or annealed at 1550°C, and those of arc melted $U_{0.85}RE_{0.15}B_2C$, were completely indexed on the basis of a rhombohedral unit cell (see Table I). Crystal symmetry ($R\bar{3}m$ as the highest symmetric space group type) and the observed intensities reveal structural

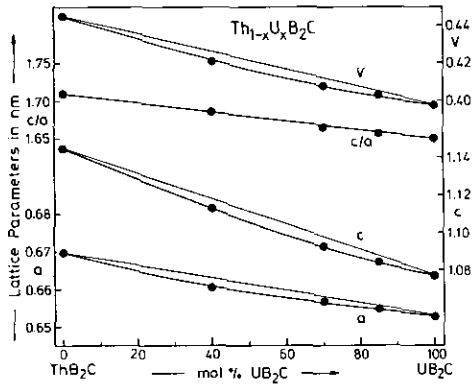

FIG. 2. Variation of unit cell dimensions in the solid solution $Th_{1-x}U_xB_2C$ as a function of the Th/U exchange.

identity with the crystal structure of ThB_2C (*4*). Figure 2 represents the variation of the unit cell volume and lattice parameters for the section $Th_{1-x}U_xB_2C$ as a function of the Th/U substitution with only slightly negative deviations from Vegard's rule. In contrast to the rather sharp X-ray patterns of the annealed alloys, those of the arc melted samples were somewhat diffuse.

It is interesting to note that the annealed samples $Th_{1-x}U_xB_2C$ for all the investigated compositions revealed the ThB_2C-type, which, for pure UB_2C, is the high temperature modification (*1*) only observed above 1675 ± 25°C; i.e., 15 mol% of ThB_2C are sufficient to stabilize the solid solution in the high temperature type, whereas heat treatment of $U_{0.85}RE_{0.15}B_2C$ for 150 hr at 1550°C in both cases, *RE* = Sc and Lu, yielded the low temperature modification of l-UB_2C. Analysis of the X-ray powder intensities of the as cast alloys $U_{0.85}RE_{0.15}B_2C$, based on the atom parameters earlier derived from a single crystal X-ray refinement of ThB_2C (*4*), proved good agreement between observed and calculated intensities, suggesting only a slight preference of the rare earth element to occupy the 3a sites in $R\bar{3}m$ over a random distribution U/*RE* in both the metal sites 3a and 6c.

3.1.4. Structural chemistry. Transition metal monoborides *T*B hitherto have been classified (*10*) as boron chain type compounds, owing to the formation of infinite zigzag boron chains. Due to steric constraints on the small octahedral voids in the monoborides of the transition metals, carbon solubilities in *T*B are exceedingly small, and except for the larger rare earth and actinoid metals no ternary *T*BC boron carbides are formed (*11*). The crystal structure of UBC has been shown (*12*) to be isopointal with the structure type of CrB with carbon atoms filling the $[U_5B]$ bipyramidal voids. Thus the crystal structures of UBC and YBC (*13*) were grouped among chain-type borides, although their B,C-nonmetal sublattices have not been properly evaluated, due to the feeble X-ray scattering power of B,C, in relation to the heavy metal atoms. Only in the structure types of ThBC (*11*) and $Th_3B_2C_3$ (*11*), boron atoms were found to deviate from boron–boron chain formation, revealing C–B–B–C units separated by a distance of 0.223 nm which seems too long in terms of strong covalent bonding.

Similarly the X-ray single crystal refinements of UBC and $UB_{0.78}C_{1.22}$ (see Section 3.1.1) did not reveal the true nonmetal sublattice, yielding merely averaged B–B distances of ca. 0.189 nm. Whatever starting parameters we used in the corresponding neutron powder refinements of $UB_{0.78}C_{1.22}$, boron atoms at 9 K as well as at 295 K unambigously revealed monoclinic symmetry. The infinite boron chain is thus dissolved into boron–boron pairs at a bonding distance of 0.1706 nm with a separation between pairs of 0.2043 nm (Table IV and Fig. 3). Each boron atom bonds to a carbon atom at a distance of 0.1553 nm as typical for a single bond type, thus forming a kinked C–B–B–C group with C–B–B and B–B–C bond angles of 112° and 121°. As seen from Table IV, the B–C distances do not vary between orthorhombic and monoclinic symmetry.

Although not proven yet in detail for recently discovered (*14*) isotypic UBN, a monoclinic B–N sublattice is inferred, resulting in kinked N–B–B–N subunits.

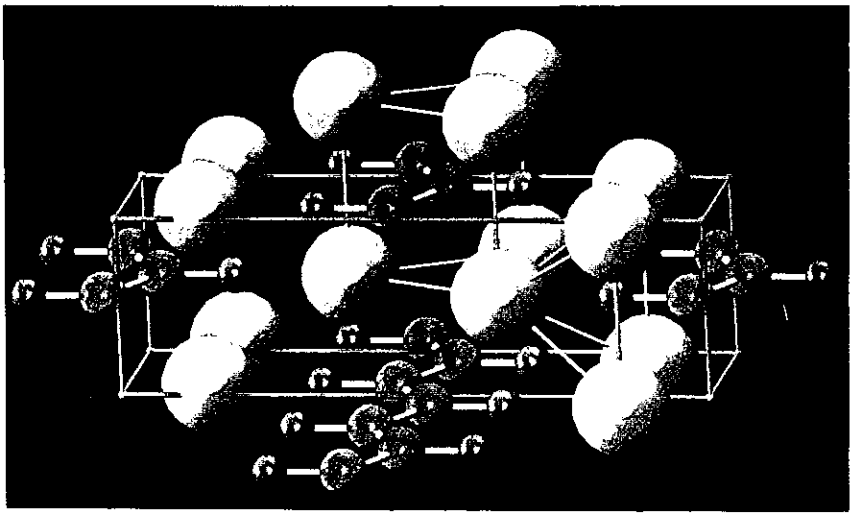

FIG. 3. Crystal structure of UBC in a three dimensional view. Large spheres are U atoms, medium sized spheres are B atoms, and small spheres are C atoms. The triangular prismatic coordination U_6B around the B atoms and the pyramidal metal coordination around the C atoms are outlined; with one additional boron atom a [U_5B] bipyramid is formed.

3.2. Magnetic Properties of $UB_{1-x}C_{1+x}$ and $U_{1-x}RE_xB_2C$ with RE = Th, Sc, Lu

Reciprocal gram susceptibilities versus temperature are presented in Figs. 4–6; the numerical results of the minimized Curie–Weiss type behavior, the type of magnetic ordering, and the corresponding transition temperatures are listed in Table I. In all cases where paramagnetic extrapolations are applicable, the temperature independent contributions to the susceptibility (χ_0) typically were in the 10^{-6} emu/g range, as usual for metallic alloy systems.

Magnetic ordering was found for all members $U_{1-x}RE_xB_2C$ with *RE* = Th, Sc, Lu (Figs. 4, 5). The variation of the interatomic distances toward lower values (Sc, Lu-substitution) or toward larger values (Th) yields qualitatively similar effects: The general result of the dilution of the uranium moments by nonmagnetic elements (Sc, Lu, Th) is a successive decrease of (a) the ferromagnetic ordering temperature (Th, Sc substitution) and (b) the saturation magnetization per uranium atom (values for 4.2 K, 18 kG are listed in Table I), while the individual paramagnetic uranium moments remain practically unaffected at a value of about 1.9(1) μ_B.

For the Lu-substituted alloy, the qualitative behavior shown in Fig. 4 is significantly different, compared to the behavior of the ferromagnetic samples. The continuous straight decrease of the magnetization vs temperature as well as the low Curie–Weiss temperature $0 \ll T_C$ and the strongly reduced saturation moment might give reason to suggest a ferrimagnetic coupling of the uranium moments. Considering the crystal structure, this assumption is not unreasonable: in the space group $R\bar{3}m$ three uranium atoms occupy the 3a position (0, 0, 0) and six uranium atoms are at 6c (0, 0, *z*, *z* = 0.31) sites. Taking the total moment of 0.65 μ_B for a parallel ordered spin system in h-UB_2C, a 1 : 2 antiparallel spin arrangement should yield a value of about 0.22 μ_B (minus a certain dilution effect). Indeed, we actually observed a value of 0.2 μ_B for the saturation $U_{1-x}Lu_xB_2C$ consistent with the above estimate.

It is interesting to note that the low tem-

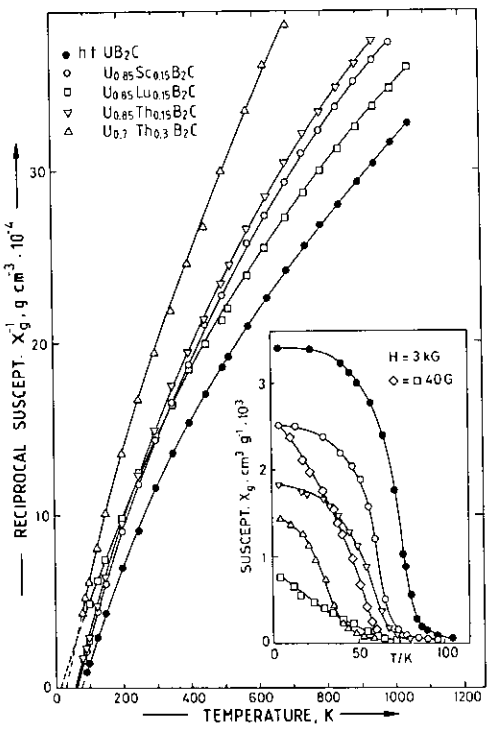

FIG. 4. Susceptibilities vs temperature for U(Lu, Sc, Th) boron carbides. In the insert the scale for the Lu-substituted compound, measured at 40 G, has to be multiplied by a factor of 10.

perature modification l-UB_2C does not exhibit any magnetic ordering; the origin of the residual ferromagnetic contribution present in this compound as well as in all of the UBC alloys is unambigously attributed to traces of incompletely transformed h-UB_2C. The ordering temperature of h-UB_2C was observed in these alloys, but the total value of the resulting magnetization was about a factor of 100 smaller, indicating an impurity level below 1% (see insert in Fig. 6). Most probably the intrinsic magnetic property of the UBC alloys is a temperature independent paramagnetism with a tendency to the onset of a weak uranium valence fluctuation behavior.

ThB_2C is weakly temperature independent paramagnetic and did not show any intrinsic ordering down to 4.2 K.

Plotting the magnetic ordering temperatures for the uranium borides, uranium carbides, and uranium boron carbides (including superconductivity of the modifications of uranium metal) versus the uranium—uranium distance in their crystal structures, we do not encounter a simple correlation of the localization and delocalization of the uranium magnetic moment as a function of the U–U distances in terms of a Hill plot with a critical distance of ca. 0.35 nm as suggested earlier (*6*), see also Fig. 7. Further studies on large single crystals are planned to get deeper insight in the interesting and peculiar magnetic behavior of UBC and l,h-UB_2C.

3.3. X-Ray Absorption Spectroscopy

Additional information on the electronic structure of uranium alloys on the borderline between localized and itinerant behavior can be derived from uranium L_3 near-edge X-ray absorption spectroscopy. The transition of $2p_{3/2}$ core level electrons into unoccupied $6d$ electronic states results in a "white" line (peak) at the L_3 absorption threshold. This resonance absorption line is weak or nearly lost in case of the rather itinerant uranium metal or in uranium intermetallic alloys with additional $5f$–$6d$ hybridization. Systems with a higher degree of localization, such as uranium oxydes or fluorides, exhibit distinct and sharper L_3-edge features (*15, 16*). In the case of rare earth elements, with a high degree of localization of their $4f$ electrons compared to the $5f$ electrons in light actinoid elements, even metallic systems exhibit distinct white lines which can be analyzed to explore mixed valence (MV) behavior in rare earth–transition metal alloys (*17*).

In Fig. 8 we compare the XANES spectra of α-uranium, UBC, $UB_{1-x}C_{1+x}$, and f.c.c. UC and UN. The spectra were analyzed by deconvoluting them into a Lorentzian line representing the discrete transition at the threshold resonance and an arctangent function describing the continuum transition (*18*). Due to the high spectrometer resolu-

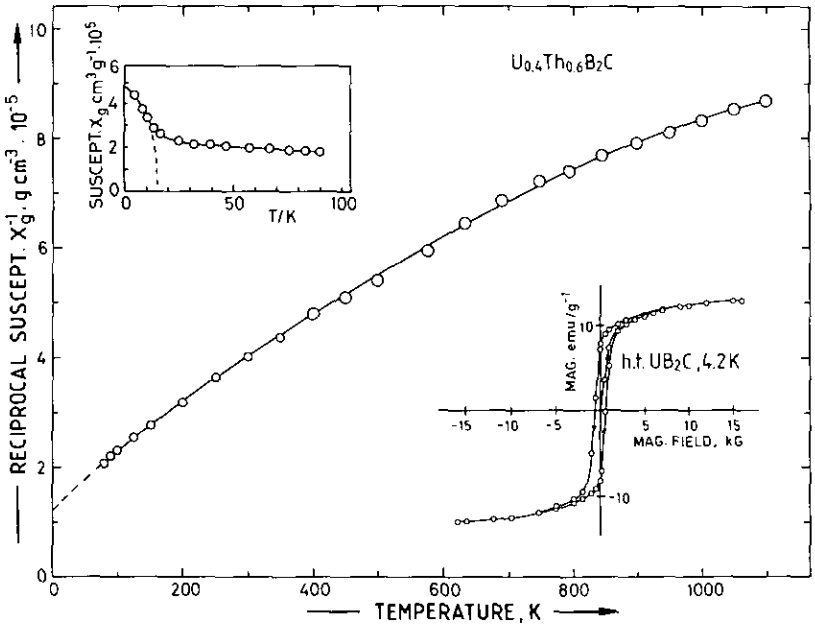

FIG. 5. Susceptibilities vs temperature for $U_{0.4}Th_{0.6}B_2C$ and magnetization loop (4.2 K) for h-UB_2C (right hand insert).

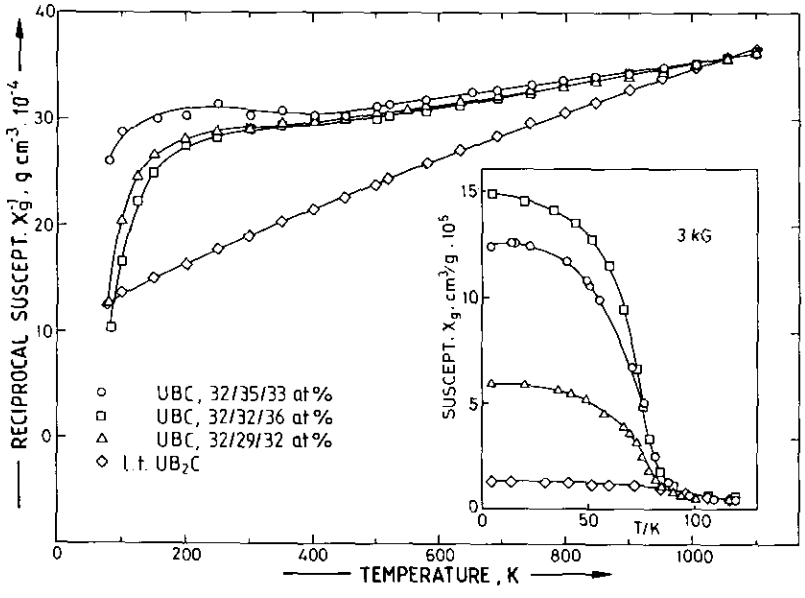

FIG. 6. Susceptibilities vs temperature for UBC alloys and for l-UB_2C. The insert shows the breakdown of magnetic ordering of the impurity phase (considered to be h-UB_2C).

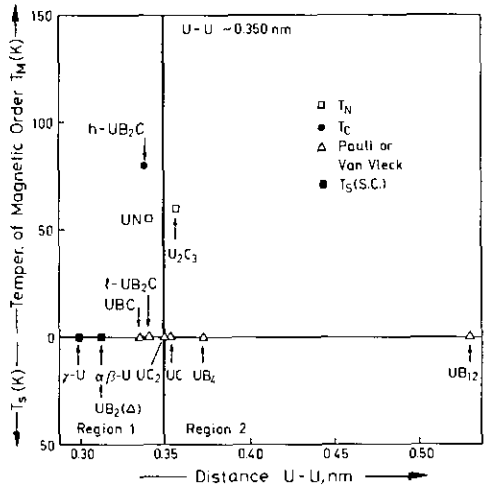

FIG. 7. Hill plot of binary and ternary U–B–C compounds.

tion compared to the $2p_{3/2}$ core hole life time, it was not necessary to fold the Lorentzian line with a Gaussian (instrumental) broadening term in order to obtain acceptable fits. The resulting values for line width, energy shift relative to α-uranium, and the relative intensity of the white line peak are listed in Table V.

From our spectra and the data presented in Table V, it is evident that little variation exists in the line width and the relative line intensity among the alloys (which themselves exhibit a distinctly sharper and more intense white line transition than α-uranium), and that their line widths and shifts are similar to those observed for uranium–transition metal alloys (*15, 19*). The changes mainly reflect a variation in the (unoccupied) $6d$ density of states from the large $6d$ bandwidth in α-uranium to the partly $5f$–$6d$ hybridized (boron) carbides displaying increased localization. XAS can thus probe the localization of electronic states in cases where magnetic data do not reveal a direct indication of localization (Fig. 6) and although UC and UBC, for example, are located in different regions of the Hill Plot (Fig. 7), they appear to have similar electronic structure as far as X-ray absorption spectroscopy can probe it. In our sample series, the highest degree of localization (i.e., the narrowest bandwidth) as inferred

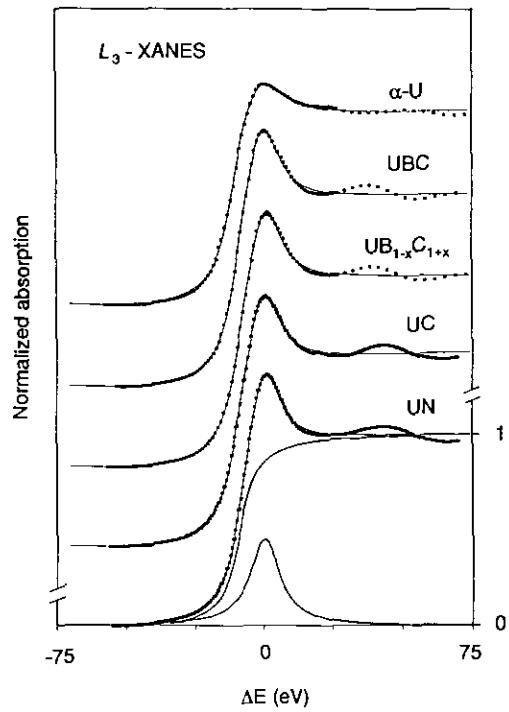

FIG. 8. L_3-XANES of uranium L_3-threshold. The zero of energy E_0 is determined by the peak position of the α-uranium white line at 17.176 keV. (This value for E_0 is about 10 eV above the inflection point of the edge spectrum (or peak in the first derivative of the spectrum) of 17.166 keV. The determination of energy shifts is more consistent and not as susceptible to line shape deviations when the peak center positions of fitted white lines are used compared to inflection points (see also Ref. *15*).) For UN, the typical deconvolution in a Lorentzian threshold resonance and an arctangent continuum transition are shown. (It should be noted that these fits are not unique with respect to the relative position of the arctangent and the Lorentzian. Similar results, proving the same qualitative trends, were obtained from fits where the center of the white absorption line lay at *lower* energies than the inflection point of the arctangent curve. A more detailed analysis involving the subtraction of the π phase-shifted L_1 edge spectra indicates that the latter description is physically more meaningful (see for example F. W. Lytle and R. B. Greegor, *Appl. Phys. Lett.* **56**(2), 192 (1990)). For consistency and better comparison with previously reported results only, we adhered in this work to the approach used in Ref. (*15–17, 19*).)

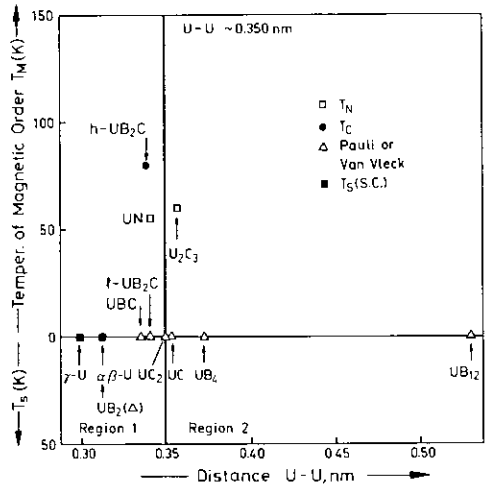

FIG. 7. Hill plot of binary and ternary U–B–C compounds.

tion compared to the $2p_{3/2}$ core hole life time, it was not necessary to fold the Lorentzian line with a Gaussian (instrumental) broadening term in order to obtain acceptable fits. The resulting values for line width, energy shift relative to α-uranium, and the relative intensity of the white line peak are listed in Table V.

From our spectra and the data presented in Table V, it is evident that little variation exists in the line width and the relative line intensity among the alloys (which themselves exhibit a distinctly sharper and more intense white line transition than α-uranium), and that their line widths and shifts are similar to those observed for uranium–transition metal alloys (*15, 19*). The changes mainly reflect a variation in the (unoccupied) 6*d* density of states from the large 6*d* bandwidth in α-uranium to the partly 5*f*–6*d* hybridized (boron) carbides displaying increased localization. XAS can thus probe the localization of electronic states in cases where magnetic data do not reveal a direct indication of localization (Fig. 6) and although UC and UBC, for example, are located in different regions of the Hill Plot (Fig. 7), they appear to have similar electronic structure as far as X-ray absorption spectroscopy can probe it. In our sample series, the highest degree of localization (i.e., the narrowest bandwidth) as inferred

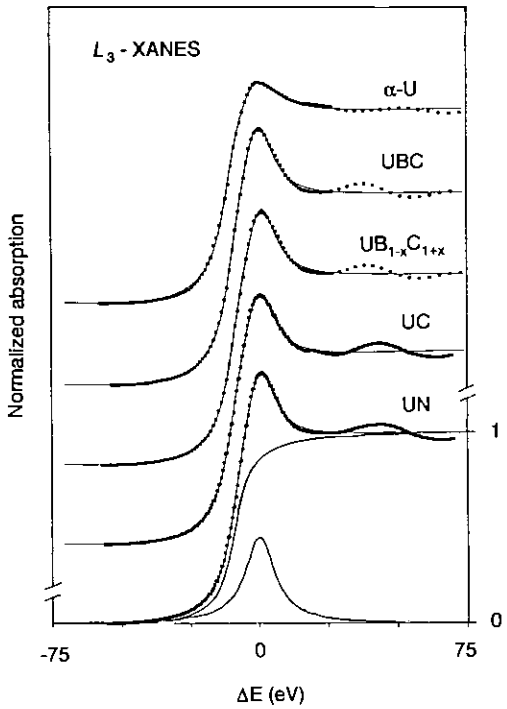

FIG. 8. L_3-XANES of uranium L_3-threshold. The zero of energy E_0 is determined by the peak position of the α-uranium white line at 17.176 keV. (This value for E_0 is about 10 eV above the inflection point of the edge spectrum (or peak in the first derivative of the spectrum) of 17.166 keV. The determination of energy shifts is more consistent and not as susceptible to line shape deviations when the peak center positions of fitted white lines are used compared to inflection points (see also Ref. *15*).) For UN, the typical deconvolution in a Lorentzian threshold resonance and an arctangent continuum transition are shown. (It should be noted that these fits are not unique with respect to the relative position of the arctangent and the Lorentzian. Similar results, proving the same qualitative trends, were obtained from fits where the center of the white absorption line lay at *lower* energies than the inflection point of the arctangent curve. A more detailed analysis involving the subtraction of the π phase-shifted L_1 edge spectra indicates that the latter description is physically more meaningful (see for example F. W. Lytle and R. B. Greegor, *Appl. Phys. Lett.* **56**(2), 192 (1990)). For consistency and better comparison with previously reported results only, we adhered in this work to the approach used in Ref. (*15–17, 19*).)

TABLE V

LEAST SQUARES FIT PARAMETERS FOR URANIUM L_3-EDGE SPECTRA

Compound	ΔE (eV)	FWHM (eV)	I (%)	ΔS (eV)
α-uranium	0.00(25)	21.21(76)	8.87	9.78(36)
UBC[a]	0.34(13)	14.64(42)	11.60	9.21(28)
$UB_{0.78}C_{1.22}$	0.57(12)	14.35(39)	10.63	9.62(25)
UC	0.44(14)	14.38(42)	10.77	9.66(30)
UN	0.21(14)	13.31(41)	10.31	9.15(21)

Note. ΔE is the energy shift with respect to α-uranium, FWHM the full width at half maximum for the Lorentzian (white line) peak, I the intensity of the Lorentzian peak relative to the edge (arctangent) jump, and ΔS the shift between the arctangent inflection point and the Lorentzian peak center (serving as a measure of consistency between the fits). The numbers in parentheses give the standard deviation σ of the last two significant digits. See Ref. (*15*) and (*19*) for additional data on intermetallic alloys.

[a] We also investigated the temperature dependence of the spectral parameters in UBC over the range of presumed valence fluctuation behavior, but no significant variations with temperature could be inferred.

from the width of the absorption line, is observed for UN which indeed exhibits type I antiferromagnetic ordering and 53 K. The ordering in UN was attributed to a large orbital-moment contribution to its $5f$ band magnetism (*20*), and the match with the prediction from the Hill plot (Fig. 7) is therefore weak.

3.4. Hydrogen Absorption in (Th, U)B_2C

Attempts to force hydrogen absorption in the (Th, U)B_2C-alloys were unsuccessful, even under hydrogen pressures as high as 70 MPa at 670 K.

Acknowledgments

This work was sponsored by the Austrian Science Foundation (Fonds zur Förderung der wissenschaftlichen Forschung in Österreich) under Contracts P8218 and P5523. Part of this work (B.R.) was performed at the Racah Institute of Physics, Jerusalem, with the kind support of the Lady Davis Fellowship Trust. The technical assistance of A. Grayevski is kindly acknowledged.

The X-ray absorption measurements at NSLS and SSRL were supported by the U.S. Department of Energy under LLNL Contract W-7405-ENG-48. Thanks are due to Joe Wong, LLNL, for his kind support and interest.

References

1. P. ROGL, J. BAUER, AND J. DEBUIGNE, *J. Nucl. Mater.* **165,** 74 (1989).
2. K. J. MATTERSON, H. J. JONES, AND N. C. MOORE, *in* "Proceedings of the 4th Plansee Seminar, Reutte/Tirol" (F. Benesovsky, Ed.) (June 1961).
3. L. TOTH, H. NOWOTNY, F. BENESOVSKY, AND E. RUDY, *Monatsh. Chem.* **92,** 794 (1961).
4. P. ROGL AND P. FISCHER, *J. Solid State Chem.* **78,** 294 (1989).
5. P. ROGL AND P. FISCHER, *J. Solid State Chem.* **90,** 285 (1991).
6. H. H. HILL, *in* "Plutonium 1970 and other Actinides" (W. N. Miner, Ed.), Nuclear Metallurgy, Vol. 17, Part I, p. 2, AIME, New York (1970).
7. J. SCHEFER, P. FISCHER, H. HEER, A. ISACSON, M. KOCH, AND R. THUT, *Nucl. Instrum. Methods Phys. Res. Sect. A* **288,** 477 (1990).
8. D. B. WILES AND R. A. YOUNG, *J. Appl. Crystallogr.* **14,** 149 (1989). [LNS/ILL-version J. Rodriguez]
9. V. F. SEARS *in* "Methods of Experimental Physics, Neutron Scattering" (R. Celotta and J. Levine, Eds.), Vol. 23, Part A, p. 52, Academic Press, Orlando, FL (1988).
10. P. ROGL, *J. Less-Common Met.* **110,** 283 (1985).
11. P. ROGL, *in* "The Physics and Chemistry of Carbides, Nitrides and Borides" (R. Freer, Ed.), Kluwer Academic, Dordrecht (1990).
12. P. ROGL, *J. Nucl. Mater.* **80,** 187, (1979).
13. J. BAUER AND H. NOWOTNY, *Monatsh. Chem.* **102,** 1129 (1971).
14. H. KLESNAR AND P. ROGL, *in* "AIP Proceedings 231 on Boron Rich Solids, Albuquerque, New Mexico" (D. Emin, Ed.), pp. 414–422 (1991).

15. G. KALKOWSKI, G. KAINDL, W. D. BREWER, AND W. KRONE, *Phys. Rev. B* **35,** 2667 (1987).
16. G. KALKOWSKI, G. KAINDL, S. BERTRAM, G. SCHMIESTER, J. REBIZANT, J. C. SPIRLET, AND O. VOGT, *Solid State Commun.* **64** (2), 193 (1987).
17. R. A. NEIFELD, M. CROFT, T. MIHALISIN, C. U. SEGRE, M. MADIGAN, M. S. TORIKACHVILI, M. B. MAPLE, AND L. E. DELONG, *Phys. Rev. B* **32,** 6928 (1985).
18. J. A. HORSLEY, *J. Chem. Phys.* **76,** 1451 (1982).
19. J. M. LAWRENCE, M. L. DENBOER, R. D. PARKS, AND J. L. SMITH, *Phys. Rev. B* **29,** 568 (1984).
20. M. S. S. BROOKS AND P. J. KELLY, *Phys. Rev. Lett.* **51,** 1708 (1983).